European Journal of Immunology

Tissue immunology and leukocyte trafficking

Basic

Research Article

CD169$^+$ subcapsular sinus macrophage-derived microvesicles are associated with light zone follicular dendritic cells

Xin Chen, Yuhan Zheng, Siming Liu, Wenjing Yu and Zhiduo Liu

Shanghai Institute of Immunology, Department of Immunology and Microbiology, State Key Laboratory of Oncogenes and Related Genes, Shanghai Jiao Tong University School of Medicine, Shanghai, China

Follicular dendritic cells (FDCs) are a specialized type of stromal cells that exclusively reside in B-cell follicles. When inflammation occurs, the FDC network is reorganized to support germinal center (GC) polarization into the light zone (LZ) and dark zone (DZ). Despite the indispensable role of FDCs in supporting humoral responses, the FDC regulatory requirements remain incompletely defined. In this study, we unexpectedly observed an accumulation of CD169$^+$ subcapsular sinus macrophage (SSM)-derived microvesicles (MVs) in the B-cell zone, which were tightly associated with the FDC network. Interestingly, a selective deposition of CD169$^+$ MVs was detected in both GC LZ FDCs in secondary follicles and on predetermined LZ FDCs in primary follicles. The ablation of CD169$^+$ MVs, resulting from SSM depletion, resulted in significantly decreased expression of LZ-related genes in FDCs. In addition, we found that CD169$^+$ MVs could colocalize with fluorescently tagged antigen-containing immune complexes (ICs), supporting a possible role of CD169$^+$ MVs in transporting antigens to the FDC network. Thus, our data reveal intimate crosstalk between FDCs and SSMs located outside B-cell follicles via SSM-released MVs, providing a novel perspective on the mechanisms underlying the regulation of FDC maturation and polarization.

Keywords: FDCs · SSMs · CD169$^+$ MVs · ICs · LZ

Additional supporting information may be found online in the Supporting Information section at the end of the article.

Introduction

Lymph nodes (LNs) are critical secondary lymphoid tissues that are strategically positioned throughout the body to filter invading pathogens or antigens draining from local tissues[1]. In addition to coordinated actions between various tightly packed immune cells, such as lymphocytes and myeloid cells, stromal cells, as a dense reticular network in LNs, play an essential role in maintaining immune homeostasis and shaping immune responses through intimate crosstalk with neighboring immune cells that helps determine the localization, activation state, and functional outcome of the latter[2]. For instance, IL-7 derived from fibroblastic reticular cells (FRCs) in the paracortical region of LNs drives the survival of naive T cells, keeping the peripheral T-cell pool at a constant level[3]. Reciprocally, the close interaction also operates as a niche to provide an influence endowed by immune cells upon stromal cells, promoting their development and proliferation, as evidenced by optimal maintenance of FRCs in inflamed LNs responding to lymphotoxin (LT) produced mainly by dendritic cells, thus facilitating the ongoing immune response[4].

Correspondence: Dr. Zhiduo Liu
e-mail: zhiduo.liu@shsmu.edu.cn

Among various types of stromal cells in LNs, follicular dendritic cells (FDCs) are known as accessory cells residing in the central region of B-cell follicles and have broad impacts on numerous aspects of B-cell biology. As a major source of CXCL13 in the steady state, FDCs help maintain an organized B-cell territory by establishing chemotactic gradients that direct CXCR5-expressing B-cell migration toward follicles upon their arrival in LNs. Once B cells enter primary follicles, FDCs constitute a highway-like cellular scaffold to guide B-cell movement, thus favoring their efficient search for cognate antigens, and secrete the B-cell trophic factor BAFF to support B-cell survival. In addition, as originally identified as 'antigen-retaining reticular cells' decades ago, FDCs are highly proficient in capturing and presenting antigen in the form of IC to B cells due to their high expression of complement receptors CD21/35 and Fc receptors, including CD23 (FcεRII) and CD32 (FcγRIIb)[5].

Upon infection or immunization, activated B cells aggregate in the secondary follicles to form a specialized structure termed the germinal center (GC) where B cells undergo somatic hypermutation (SHM), clonal expansion and selection that ultimately lead to the generation of high affinity antibody-secreting plasma cells and memory B cells[6]. The precision and efficacy of the actions of these events lie in a further segregation of GC into two distinct compartments known as the light zone (LZ) and dark zone (DZ), with each favoring a portion of the assignments but integration of the two accounting for a full GC development. Remarkably, this delicate division of labor in two distinct microenvironments is coincidentally matched by remodeling of the FDC network into two diverse populations residing in the LZ and DZ. LZ FDCs acquire a further mature phenotype relative to the ones in primary follicles and DZ, exhibiting the expression of more abundant complement receptors, Fc receptors and integrin ligands that correspond to their role as antigen trapping and presenting cells in LZ. Furthermore, LZ and DZ FDCs adopt different chemokine expression profiles tailored for the regulation of GC B-cell retention within and orchestrated trafficking across the two zones [7, 8]. Hence, the heterogeneity in the gene expression profile and the resultant functional specification of FDC compositions underpin their pivotal contributions to humoral immunity. Despite the tight correlation between FDCs and antibody responses, how the immunobiology of FDCs is regulated remains largely unknown. Part of the reason for this insufficiency comes from the fact that the only currently known cells that FDCs can interact with are B cells due to the highly constrained localization of FDCs. Therefore, the exploration of additional cellular candidates that can target FDCs would be of vital importance for understanding the establishment of a supportive stromal microenvironment for robust B-cell responses.

Subcapsular sinus macrophages (SSMs) are specialized lymph node macrophages that strategically localize at the interface of the resident lymphohematopoietic system and circulating fluid[9]. CD169 (also known as sialoadhesin or Siglec-1), which recognizes sialylated pathogens[10, 11], is highly expressed on and often regarded as a specific marker of SSMs. In accordance with their unique positioning in close proximity to afferent lymphatic drainage, SSMs are considered gatekeepers in LNs, in that they can prevent viruses from undergoing systemic dissemination by capturing and retaining them locally[12–14]; they can acquire and present lymph-borne particulate antigens to underlying follicular B cells to trigger immune responses[15–17]; and they are able to activate innate-like lymphocytes, NK cells and iNKT cells that accumulate in the sinus upon infection or stimulation[18–20]. However, the actions of SSMs outside the subcapsular sinus floor remain undefined.

Here, using confocal imaging and correlative light and electron microscopy, we observed that SSM-derived CD169$^+$ microvesicles (MVs) were closely associated with FDCs in B-cell follicles. Furthermore, we detected a preferential deposition of CD169$^+$ MVs on LZ FDCs, as FDCs associated with CD169$^+$ MVs had higher expression levels of LZ FDC signature genes in both secondary and primary follicles. Elimination of CD169$^+$ MVs by SSM depletion led to the downregulation of genes related to LZ FDCs. Altogether, our study establishes a strong link between SSMs and FDCs, providing insight into the complex regulation of humoral responses.

Results

CD169$^+$ microvesicles are associated with FDCs in B-cell follicles

SSMs are generally localized at the periphery of LNs, as indicated by immunofluorescence staining for CD169, a specific surface marker on SSMs (Figure 1A). Intriguingly, however, we also observed clear CD169 signals inside B-cell follicles. The CD169 signals exhibited a stretching dendrite-like distribution pattern, suggestive of a strong association with stromal network versus round-shape lymphocytes. Indeed, those CD169 signals colocalized intimately with CD35$^+$ FDCs that resided at the center of B-cell follicles. This close association was further confirmed by staining for other FDC markers, including CD16/32, FDC-M1, and VCAM-1 (Figure 1B). Notably, the colocalization could be observed in the spleen and multiple types of LNs (supplementary Figure S1), indicating that it is a universal phenomenon in secondary lymphoid organs. The specificity of CD169 staining was verified, as such signals were not detected usingCD169$^{DTR/DTR}$ mice, in which a cassette encoding human diphtheria toxin receptor (DTR) was inserted into the *Siglec1* gene locus in both alleles, resulting in the disruption of the coding sequence and a loss of CD169 expression[21]. Additionally, the staining with two anti-CD169 monoclonal antibodies that recognize distinct epitopes on CD169 exhibited the same distribution pattern of CD169 signals (supplementary Figure S2).

Because CD169 is mainly expressed by tissue resident macrophages, we considered the possibility of CD169$^+$ macrophages in follicles. As shown in Figure 1C, however, confocal imaging analysis revealed that CD169$^+$ signals barely overlapped with cells expressing the reporter gene tdTomato in LNs from either LysMCre-RosaTdT or Ms4a3Cre-RosaTdT mice, in which myeloid cells and monocyte-derived cells could be

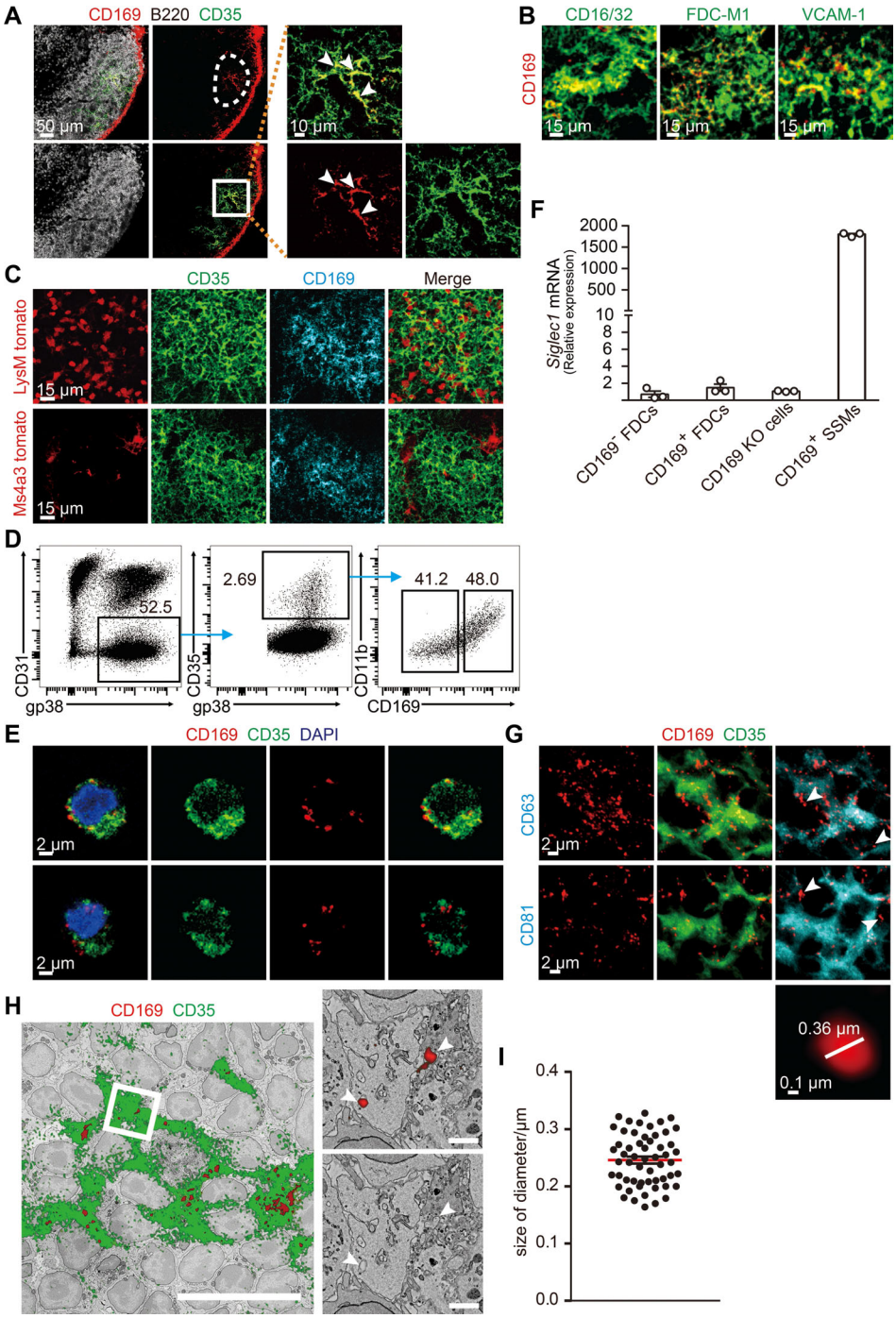

Figure 1. CD169⁺ MV deposition on FDCs. (A) Immunofluorescence (IF) staining of inguinal lymph node (iLN) sections. The white dashed line indicates CD169 signals inside B-cell follicles. The boxed region is enlarged in the right panel, and arrowheads indicate representative CD169 signals associated with the FDC network. (B) Representative IF images of iLN sections showing staining for CD169 (red) and FDC markers (green), including CD16/32, FDC-M1 and VCAM-1. (C) Representative IF images of iLN sections from LysMCre-RosaTdT mice and Ms4a3Cre-RosaTdT mice. (D) Detection of CD169 on FDCs. Representative flow cytometry plots showing the gating strategy of FDCs ($gP38^+CD31^-CD35^+$) isolated from peripheral LNs (gated on $CD45^-$). Numbers adjacent to outlined areas indicate the percentages of cells in each area. (E) Representative IF images of sorted $CD45^-gp38^+CD31^-CD35^+$ FDCs fixed on slides. (F) *Siglec1* mRNA quantification by qPCR in $CD169^+$ FDCs, $CD169^-$ FDCs, CD169 KO cells and $CD169^+$ SSMs normalized to *18S rRNA*. The graphs show the mean ± SEM of 1 representative from 3 independent experiments. (each sample was pooled from peripheral LNs of 6 mice, n = 3) (G) High-resolution IF images of iLN sections captured by the ZEISS Airyscan module showing staining for CD63 and CD81, with a representative CD169 signal in an enlarged view showing its diameter as 0.36 μm. Arrowheads indicate scattered CD169 signals associated with FDCs. (H) Representative CLEM alignment of LM images with EM images of iLN sections. The boxed region in the left panel (scale bar, 15 μm) is enlarged in the right panel (scale bar, 1 μm). Arrowheads indicate representative structures of CD169 signals under 2 nm resolution. (I) Measurement of the diameters of CD169 signals in EM images (each dot represents one CD169 signal, and 56 dots are shown as the mean ± SEM). The red line represents the mean value. All the representative imaging data shown were from 3 independent experiments.

labeled, respectively, while SSMs, tingible body macrophages and monocytes were all tdTomato positive, as expected. These data indicate that $CD169^+$ signals in B-cell follicles did not represent macrophages originally located in the follicle or migrating from outside. To further study FDC-associated CD169 signals, we next isolated FDCs ($CD45^-GP38^+CD31^-CD35^+$) from LNs for analysis. Consistent with imaging data of LN sections, flow cytometric analysis clearly showed the presence of a fraction of $CD169^+CD11b^{hi}$ FDCs (Figure 1D), and the CD169 signals could be detected in sorted FDCs by IF ex vivo (Figure 1E), a result suggesting a possibility of CD169 expression directly by FDCs, given the previous reports also showing that certain types of cells, including DCs and monocytes, could upregulate CD169 expression upon stimulation [22, 23]. To test this idea, CD169 transcripts in sorted FDCs were measured by qPCR. In contrast with the abundant expression in $CD169^+$ SSMs, CD169 mRNA was undetectable in both $CD169^+$ FDCs and $CD169^-$ FDCs at a level equivalent to that of cells isolated from CD169 KO mice, strongly indicating that FDCs did not express CD169 but obtained CD169 signals from other cells (Figure 1F).

We then visualized the CD169 signals using superresolution imaging and found that they were mainly composed of dot-like fluorescence, with a size much smaller than that of a regular cell (Figure 1G), which suggests they may represent extracellular vesicles (EVs). EVs are nanometer-scale particles that mediate efficient intercellular communication via the cargo they carry and can be divided into three types based on their size: exosomes (40 nm–120 nm in diameter), microvesicles (100 nm to 1,000 nm in diameter) and apoptotic bodies (500 nm–2 μm in diameter)[24]. Superresolution imaging revealed that the size of most CD169 signals was within the range of 100–500 nm in diameter (figure 1G), similar to that of microvesicles. In addition, staining for CD63 and CD81, two classical markers of exosomes, revealed no colocalization with CD169 signals (Figure 1G), ruling out the possibility of CD169 signals as exosomes. As reported[25], FDCs expressed high levels of CD63 and CD81. In further efforts to visualize the delicate structures of the blebs, we utilized correlative light and electron microscopy (CLEM), which allowed us to identify the region of interest (ROI) by light microscopy (LM) and to subsequently analyze the ultrastructural details by high-resolution electron microscopy (EM). The alignment of the images clearly identified CD35$^+$ FDC dendrites stretching among the extracellular space of densely packed lymphocytes. A good overlay of CD169 fluorescent signals and spherical bleb-like structures was observed, despite the inevitable resolution gap between and different distortions in the two techniques. The majority of CD169$^+$ blebs were found attached to or inside FDCs, with an average diameter of approximately 250 nm (Figure 1H, I), indicating that they were MVs. Consistent with the CLEM data, flow cytometric analysis indicated that aside from surface positioning, CD169$^+$ signals were also detected inside FDCs (supplementary Figure S3). Taken together, CD169$^+$ MVs can associate with FDCs inside B-cell follicles.

CD169$^+$ MVs derived from SSMs increase with age

The current findings prompted us to study the cellular source of CD169$^+$ MVs that could be deposited on the FDC network. SSMs highly express CD169 and reside underneath the subcapsular sinus that encircles B-cell follicles, making them a prime candidate. Therefore, we sought to examine our hypothesis using CD169 $^{DTR/+}$ mice, in which DTR expression from one allele allows for transient and selective depletion of CD169$^+$ cells upon diphtheria toxin (DT) administration, whereas the other intact allele permits normal CD169 expression[21]. One day after DT injection, the majority of SSMs (CD11c^{int}CD169^{hi}) were depleted, while CD169$^+$ MVs remained attached to the FDC network without a discernable decrease (Figure 2A, B), a result further validating our previous findings that FDC-associated CD169 signals did not represent intact macrophages and that FDCs did not express CD169, or they both would be depleted otherwise. Continuous SSM depletion with DT injection every 3 days for 2 weeks, however, led to CD169$^+$ MV elimination (Figure 2A, B, C), demonstrating that CD169$^+$ MVs derived from SSMs can stay associated with FDCs for a substantial period of time.

Next, we examined the developmental dynamics of FDC-associated CD169$^+$ MVs by assessing LNs isolated from mice at different times after birth. As shown in Figure 2D and 2E, the colocalization of FDCs with CD169$^+$ MVs was negligible until 3 weeks and became evident at 4 weeks, followed by a marked increase thereafter. Collectively, SSM-derived CD169$^+$ MVs associate with FDCs and increase with age.

FDCs associated with CD169$^+$ MVs resemble LZ FDCs in inflamed LNs

Inflammation induces the recruitment of activated B cells into follicles to form GCs, which comprise the LZ and DZ, and the reticular microenvironments in these two compartments differ to support GC B-cell selection. To investigate the possible positioning of CD169$^+$ MVs in GC, we immunized mice with KLH/CFA subcutaneously, and the draining LNs were harvested at day 7 for imaging analysis. Within the GC area demarcated by Ki67 staining, CD169$^+$ MV-associated FDCs were CD35^{hi} that mainly resided at the pole of the GC proximal to the subcapsular sinus, corresponding to LZ FDCs (Figure 3A). To verify this, CD23 staining was used to define LZ FDCs[5]. As shown in Figure 3B, CD169 signals predominantly colocalized with CD23$^+$ FDCs, and the intensity of CD169 signals decreased progressively along the length of GC toward the T-B border, correlating with similar biased distribution patterns of CD35 and CD23 signals. Complementary to the imaging analysis, we additionally sorted CD169$^+$ FDCs (FDCs associated with CD169$^+$ MVs) and CD169$^-$ FDCs (FDCs not associated with CD169$^+$ MVs) for LZ/DZ-related gene expression measurement. CXCL13 and CXCL12 are signature chemokines produced by LZ and DZ FDCs, respectively, for the guidance of B-cell migration within GCs. qPCR analysis showed that *Cxcl13* was markedly elevated in CD169$^+$ FDCs, whereas an increase in *Cxcl12* expression was detected in CD169$^-$ FDCs. Consistent with histological analysis, *Cr2* (encoding CD35) transcripts were also significantly upregulated in CD169$^+$ FDCs compared with CD169$^-$ FDCs (Figure 3C). Thus, CD169$^+$ MVs preferentially interact with LZ FDCs in secondary follicles.

To further dissect the molecular identity of the two FDC subsets, RNA-seq was performed on sorted CD169$^+$ FDCs and CD169$^-$ FDCs from immunized mice. The transcripts of LZ-associated genes (*Fcer2a*, *Fcgr2b*, *Coch*, *Cr2*, *Pthln*, *Cxcl13*, etc.) were elevated, while the expression levels of DZ-associated genes (*Pdlim3*, *Efemp2*, *Raly*, *Trf*, *Cxcl12*, etc.) were downregulated in CD169$^+$ FDCs compared to CD169$^-$ FDCs (Figure 3D). Interestingly, we found an enrichment of MRC-related genes with higher expression in CD169$^+$ FDCs in comparison to a concentration of TBRC-associated genes with more abundant transcripts in CD169$^-$ FDCs (Figure 3D). Given the topology of the stromal cell network in B-cell follicles, these data suggest a closer gene expression relationship between the neighboring reticular subsets. Gene ontology analysis of upregulated genes in CD169$^-$ FDCs revealed

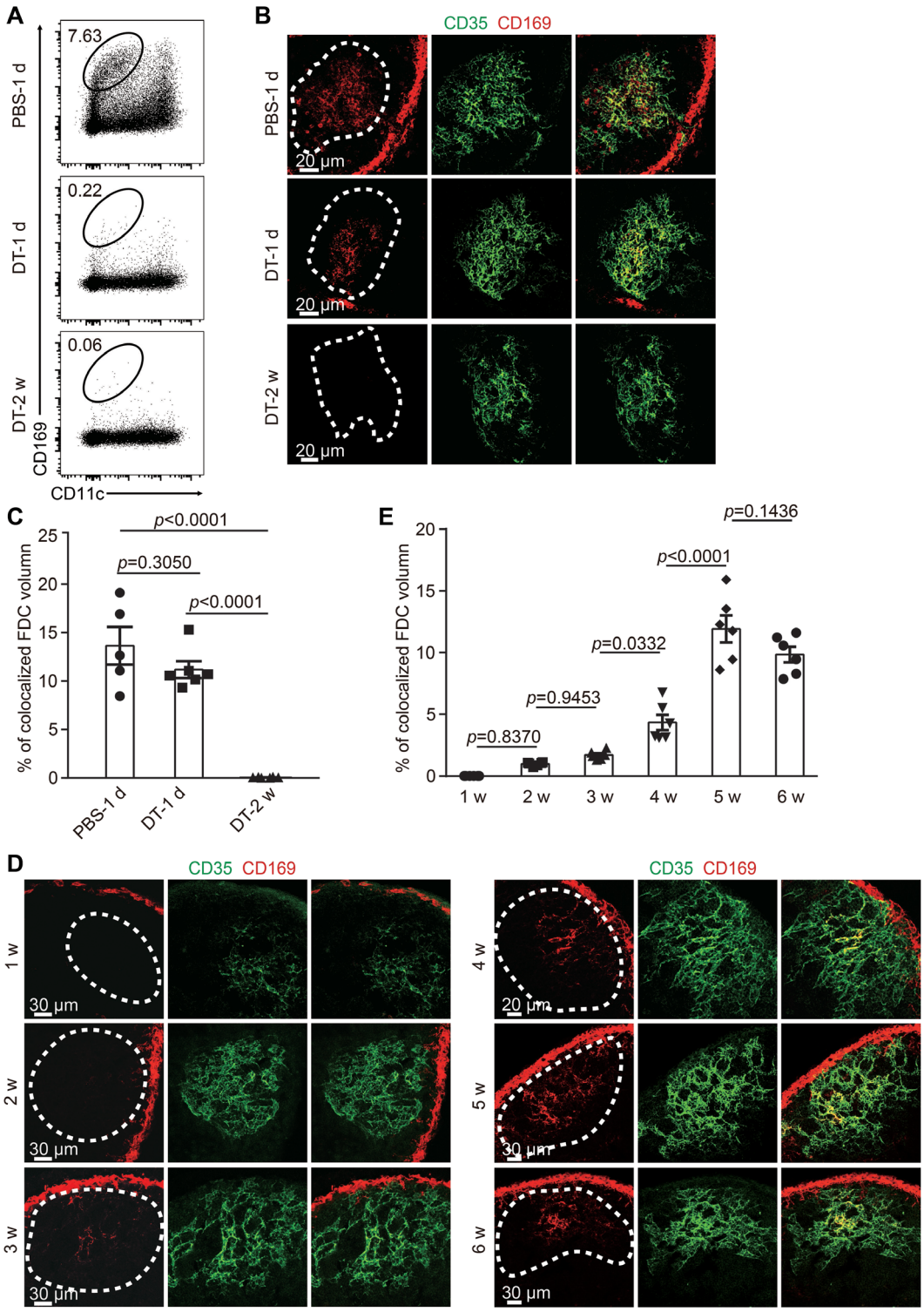

Figure 2. SSM-derived CD169$^+$ MVs increase with age. (A-C) CD169-DTR mice were treated with PBS or DT. For the DT-2 week group, DT was intraperitoneally injected every 3 days. iLNs were harvested at indicated time points for analysis. (A) Representative flow cytometry plots showing CD11c^{int}CD169^{hi} SSMs (gated on CD3$^-$B220$^-$) from iLN. Numbers adjacent to outlined areas indicate the percentages of cells. (B) Representative IF images of iLN sections. FDC networks are encircled by the white dashed lines. (C) Quantification of the percentage of FDC volume colocalized with CD169$^+$ MVs in panel (B). The graph shows the mean ± SEM of 5–6 iLNs from 3 mice per group. Each symbol represents an individual iLN. The exact *P* values from one-way ANOVA are shown. (D-E) Kinetic analysis of CD169$^+$ MVs in iLNs as age increases. (D) Representative IF images of iLN sections from mice aged from 1 to 6 weeks. FDC networks are encircled by the white dashed lines. (E) Quantification of the percentage of FDC volume colocalized with CD169$^+$ MVs at the indicated ages. The graph shows the mean ± SEM of 5–6 iLNs from 3 mice per group. Each symbol represents an individual iLN. The exact *P* values from one-way ANOVA are shown. The representative data in (A-E) were from 3 independent experiments.

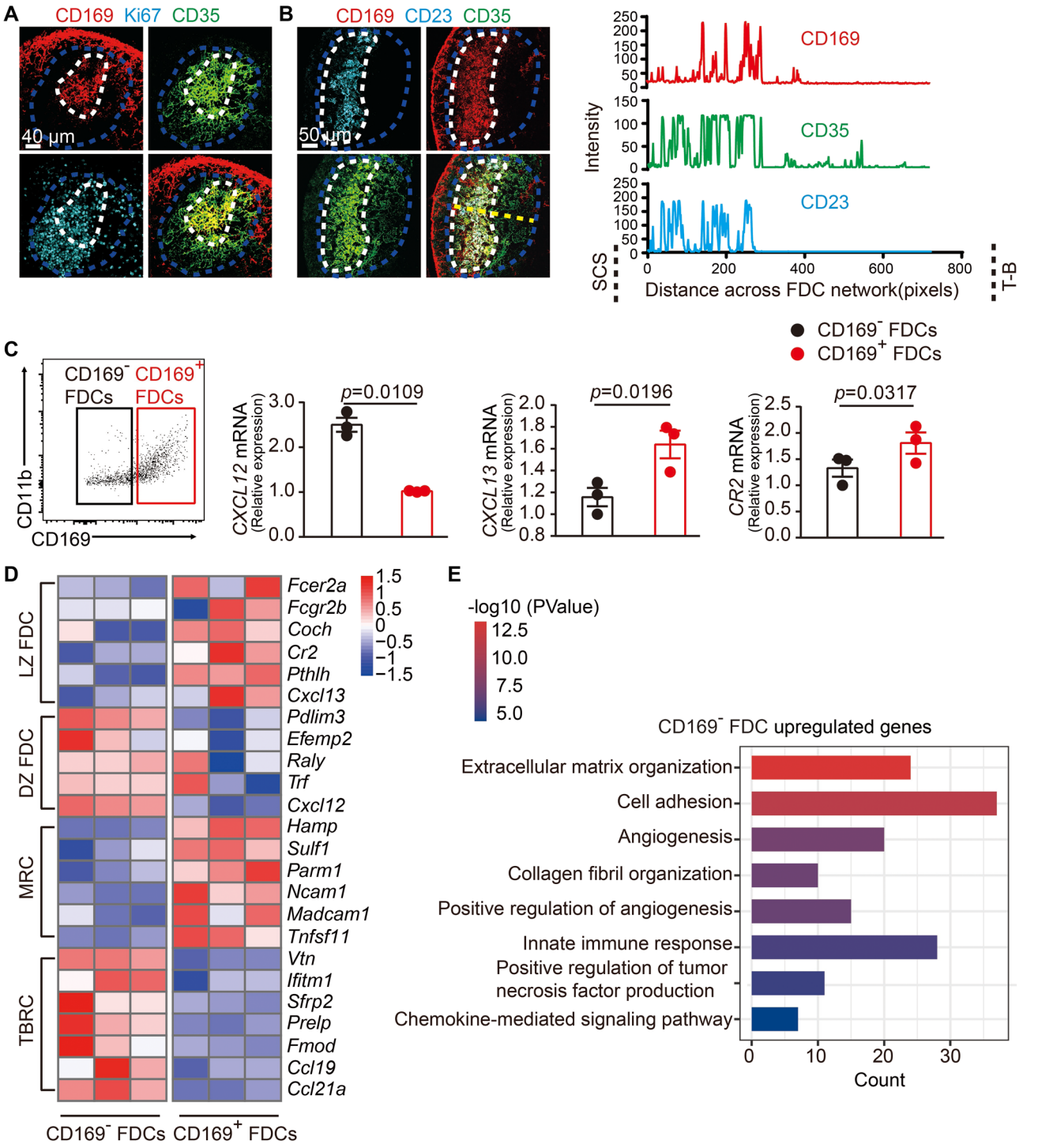

Figure 3. CD169⁺ FDCs resemble LZ FDCs in inflamed LNs. The mice were immunized with KLH in CFA s.c. for 7 days (multisite immunization). (A-B) Representative IF images of draining iLN sections from immunized mice. The blue and white dashed lines indicate the perimeter of FDC networks and CD169⁺ MV areas, respectively. (B) The yellow dashed line from the SCS to the T-B border indicates the axis of CD169, CD35 and CD23 intensity measurement in the right panel. Representative images in (A-B) were from 3 independent experiments. (C) mRNA quantification of *Cxcl12*, *Cxcl13* and *Cr2* normalized to *18S rRNA* by qPCR in sorted CD169⁻ FDCs and CD169⁺ FDCs from immunized mice (The gating scheme of CD169⁻ FDCs and CD169⁺ FDCs are shown in the left panel). The graphs show the mean ± SEM. of 1 representative from 3 independent experiments (each sample was pooled from peripheral draining LNs of 6 immunized mice, n = 3). The exact *P* values from the two-tailed *t* test are shown. (D-E) CD169⁻ FDCs and CD169⁺ FDCs from immunized mice were sorted for RNA seq analysis (each sample was pooled from draining peripheral LNs of 6 immunized mice, n = 3). (D) Heatmap of the scaled gene expression of LZ and DZ FDC markers and curated genes, including MRC genes and TBRC genes shown for CD169⁻ FDCs and CD169⁺ FDCs. (E) Bar plot showing gene ontology (GO) analysis of upregulated differentially expressed genes (DEGs) in CD169⁻ FDCs versus CD169⁺ FDCs. The analysis was performed using DAVID. Genes with an adjusted *P* value < 0.05 and a fold change > 1.5 were used.

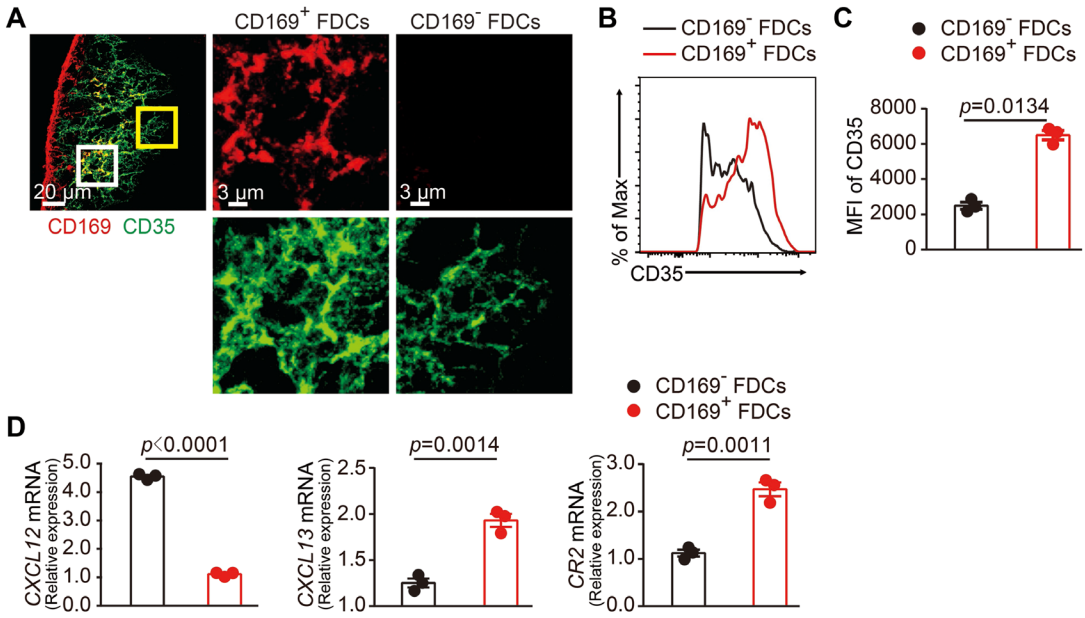

Figure 4. CD169⁺ FDCs resemble LZ FDCs in LNs in the steady state. (A) Representative IF images of iLN sections from unimmunized mice with magnified views of CD169⁺ FDCs and CD169⁻ FDCs indicated by white and yellow boxes, respectively. One representative from three independent experiments is shown. (B) Representative histogram plot showing the relative expression of CD35 in CD169⁺ FDCs and CD169⁻ FDCs from unimmunized mice. (C) Quantification of the mean fluorescence intensity (MFI) of CD35 in CD169⁺ FDCs and CD169⁻ FDCs by flow cytometry in (B). (D) mRNA quantification of *Cxcl12*, *Cxcl13* and *Cr2* normalized to *18S rRNA* by qPCR in sorted CD169⁺ FDCs and CD169⁻ FDCs from unimmunized mice. The graphs in (C-D) show the mean ± SEM of 1 representative from 3 independent experiments (each sample was pooled from peripheral LNs of 10 naive mice, n = 3). The exact *P* values from the two-tailed *t* test are shown.

deep involvement in a series of biological processes, such as the innate immune response and cell adhesion. Particularly, in line with a previous report showing higher expression of matrix components in DZ FDCs[7], a significant enrichment of the upregulated genes related to extracellular matrix organization (*Col1a2*, *Col3a1*, *Mmp2*, *Ecm2*, *Vtn*, etc.) was identified in CD169⁻ FDCs (Figure 3E). Taken together, these data indicate that CD169⁺ FDCs resemble LZ FDCs, whereas CD169⁻ FDCs are similar to DZ FDCs in inflamed LNs.

CD169⁺ MVs are associated with LZ FDCs in naive LNs

Despite the homeostatic maintenance of FDC abundance in LNs, recent single-cell sequencing-based studies revealed heterogeneity in the FDC composition, with predetermined LZ/DZ FDC subsets present even in the steady state[7]. Then, we asked whether a selective association between CD169⁺ MVs and the LZ FDC subset also occurs in unimmunized primary follicles. Noticeably, in LNs from untreated mice, we observed that CD169⁺ MVs were preferentially deposited on FDCs with bright CD35 staining, in contrast to the relatively dim CD35 signals on cells without CD169⁺ MVs (Figure 4A), which was further confirmed by flow cytometric analysis of sorted FDCs (Figure 4B, C). Moreover, the expression patterns of LZ/DZ-associated signature genes in CD169⁺ and CD169⁻ FDCs isolated from untreated mice were similar to those from immunized mice, in that *Cxcl13* and *Cr2* transcripts were higher while *Cxcl12* transcripts were lower in CD169⁺ FDCs than in CD169⁻ FDCs (Figure 4D). In summary, CD169⁺ MVs associate with LZ FDCs in primary follicles, suggesting a possible role of CD169⁺ MVs in the regulation of the FDC phenotype.

Long-term ablation of SSMs alters the FDC phenotype

To explore the potential impacts of SSMs and CD169⁺ MVs on FDCs, we treated naive mice with clodronate to achieve local ablation of SSMs in popliteal lymph nodes (pLNs). Two weeks post-clodronate administration, along with SSM disruption, the majority of CD169⁺ MVs in B-cell follicles vanished, while GC B-cell development was not detected (supplementary Figure S4). Quantification of imaging data revealed a marked decrease in CD35 and CD16/32 expression levels in FDCs in LNs with clodronate treatment compared with FDCs in control LNs (Figure 5A, B). Next, we performed RNA-seq to provide deeper insight into the gene expression profiles of FDCs. In comparison to control FDCs, FDCs from clodronate-treated LNs showed reduced expression of genes related to LZ FDCs, including *Fcer2a*, *Fcgr2b*, *Coch*, *Cr2*, *Homer2*, *Postn*, and *Tmem119*, but expressed higher levels of genes encoding extracellular components, which have been reported to be elevated in DZ FDCs (Figure 5C). Together, these results demonstrate that long-term depletion of SSMs, which results in CD169⁺ MV ablation, could affect FDC maturation in primary follicles. To distinguish whether the ablation of SSMs or CD169⁺ MVs led to a change in FDC phenotype, we assessed FDCs in naive mice treated with clodronate for 4 days or 7 days, in

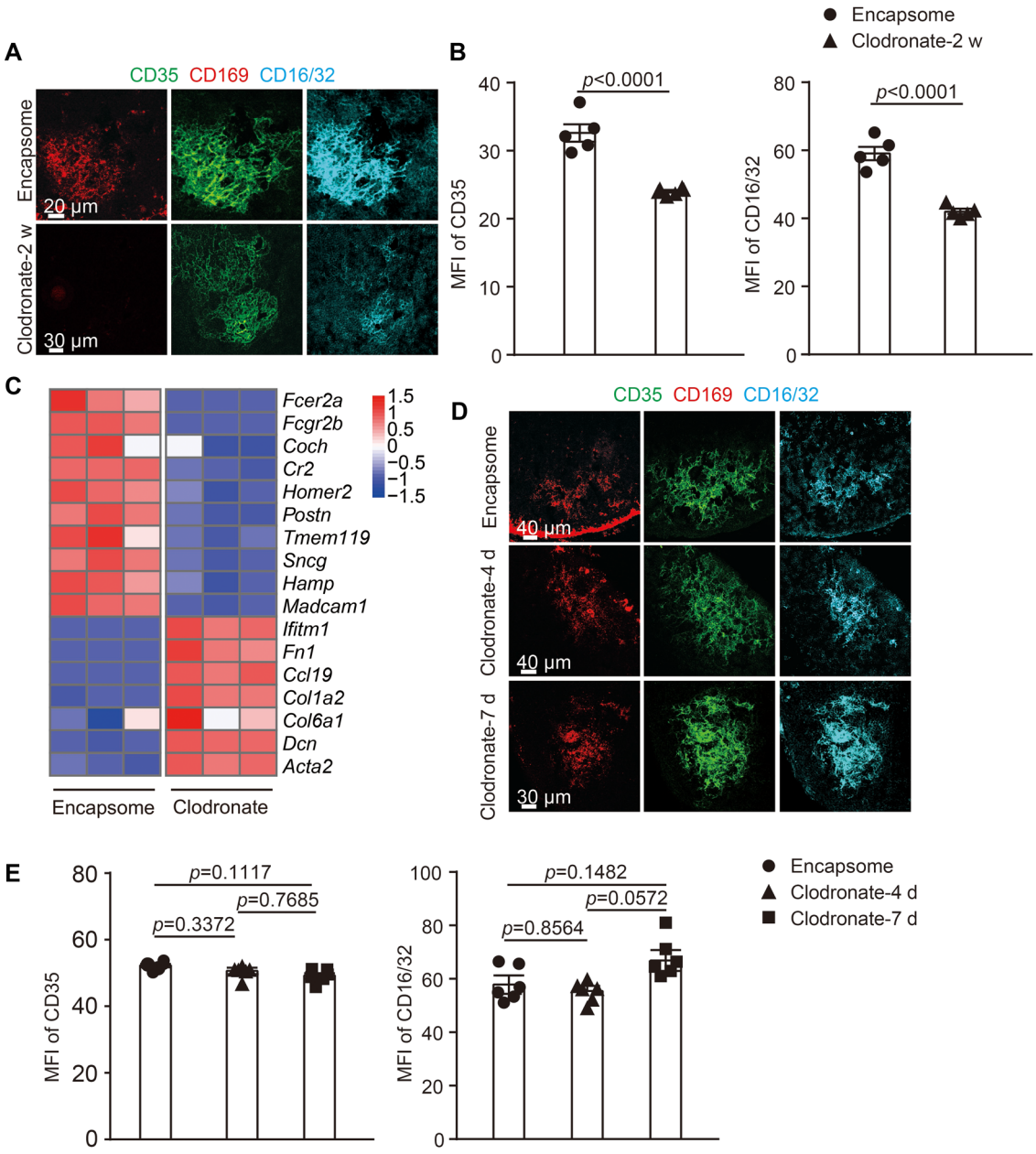

Figure 5. SSMs may influence FDC maturation by shedding CD169⁺ MVs. (A) Representative IF images of popliteal lymph node (pLN) sections from encapsome- or clodronate-treated mice. Encapsome or clodronate was injected f.p. every 7 days for 2 weeks. (B) Quantification of the mean fluorescence intensity (MFI) of CD35 and CD16/32 in (A). The graph shows the mean ± SEM of 5–6 pLNs from 3 mice per group. Each symbol represents an individual pLN. The exact *P* values from the two-tailed *t* test are shown. (C) FDCs from encapsome or clodronate treated mice were sorted for RNA seq analysis (each sample was pooled from pLNs of 20 mice, n = 3). Heatmap of the scaled gene expression of curated genes shown for sorted CD45⁻gP38⁺CD31⁻CD35⁺ FDCs from mice treated with encapsome or clodronate for 2 weeks. (D) Representative IF images of pLN sections from encapsome or clodronate-treated mice. pLNs were harvested 4 or 7 days post-injection as indicated. (E) Quantification of the MFI of CD35 and CD16/32 in (D). The graph shows the mean ± SEM of 5–6 pLNs from 3 mice per group. Each symbol represents an individual pLN. The exact *P* values from one-way ANOVA are shown. The representative data in (A-B) and (D-E) were from 3 independent experiments.

which SSMs were depleted while CD169⁺ MVs remained associated with FDCs. As shown in Figure 5D and 5E, FDCs exhibited comparable levels of CD35 and CD16/32 among the control, clodronate-4 day, and clodronate-7 day groups, suggesting that CD169⁺ MVs derived from SSMs are required for the regulation of FDC maturation.

CD169⁺ MVs may facilitate IC transfer to FDCs

Soluble antigens with smaller molecular weights can diffuse rapidly through conduits and be trapped by FDCs directly[26], while lymph-borne particulate antigens are captured by SSMs and transferred to FDCs via noncognate B cells in the form of ICs[9,

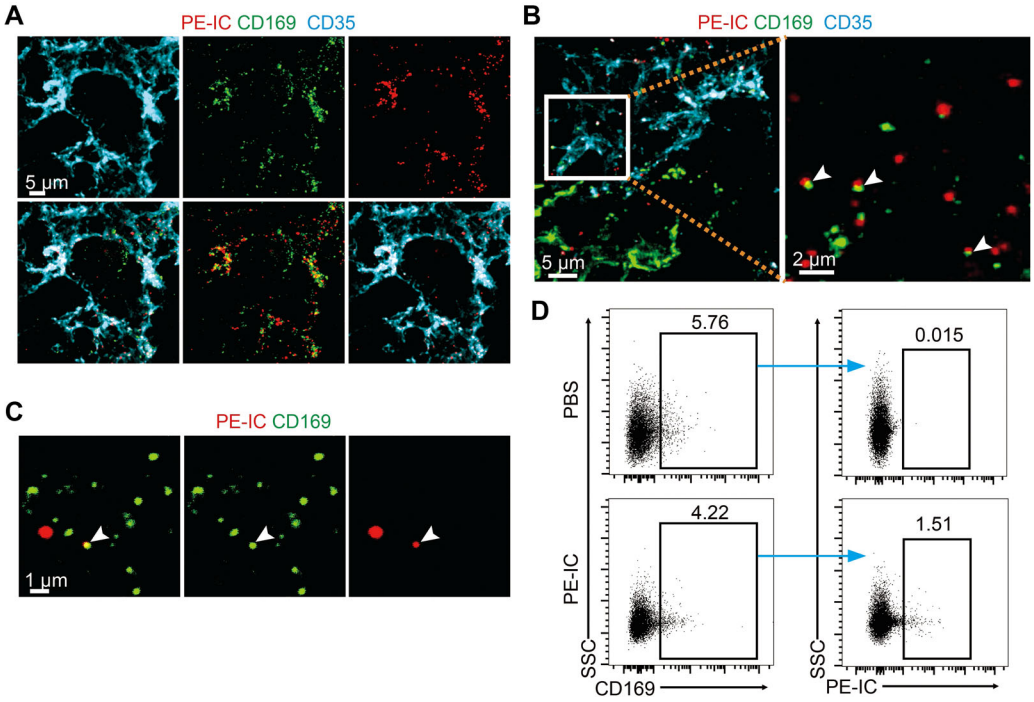

Figure 6. Colocalization of PE-ICs and CD169⁺ MVs. Mice were passively immunized with PE-ICs by injecting rabbit IgG anti-PE (i.p.) and PE (s.c.). iLNs were harvested 12 h post-PE injection. (A-B) Representative IF images of draining iLN sections. (B) Arrowheads in the magnified view of the boxed region indicate representative colocalization of PE-ICs and CD169⁺ MVs in vivo. (C) Representative IF images of isolated MVs from PE-IC-immunized mice. Twelve hours post-PE injection, MVs from draining iLNs were isolated through sequential ultracentrifugation, stained and fixed on slides. The arrowhead indicates PE-IC associated with isolated CD169⁺ MV. (D) Representative flow cytometry plots showing PE-IC labeling on isolated CD169⁺ MVs in PE-IC-immunized mice compared with PBS-treated mice (each sample was pooled from peripheral LNs of 6 mice). Numbers adjacent to outlined areas indicate the percentages of MVs. The representative data in (A-D) were from 3 independent experiments.

27, 28]. Our findings of substantial deposition of SSM-derived CD169⁺ MVs on FDCs raise the possibility that CD169⁺ MVs could also serve as antigen carriers in addition to B-cell-dependent antigen relays. To explore this, mice were sequentially injected with antibody to R-phycoerythrin (PE) and PE for the generation of fluorescently tagged ICs in vivo. In draining LNs 12 hours post-PE injection, abundant PE-ICs were deposited on FDCs, highly correlating with CD169⁺ MV distribution (Figure 6A). A higher magnification view of the FDC area clearly showed the colocalization of individual CD169⁺ MVs and PE-ICs in situ (Figure 6B). To further study their correlation, MVs were isolated from IC-injected LNs via sequential ultracentrifugation, which removed intact cells and cell debris. PE-IC binding was detected on a portion of isolated CD169⁺ MVs by both IF (Figure 6C) and flow cytometry (Figure 6D). Together, these results demonstrate the close association between CD169⁺ MVs and ICs, suggesting a possibility that CD169⁺ MVs could facilitate the delivery of ICs to FDCs.

Discussion

FDCs are essential reticular cells residing in follicles to support B-cell functions, and the nature of FDCs is in turn largely shaped by various inputs from neighboring B cells, the only known cells that interact with FDCs to date. Our study demonstrates novel crosstalk between FDCs and SSMs, which could potentially affect FDC maturation and the outcomes of humoral responses.

SSMs have been reported to undergo disruption upon inflammation by responding to pathogen-associated molecular patterns (PAMPs), such as CPG or LPS[15]. Our observation that a large quantity of SSM-derived CD169⁺ blebs associated with FDCs first led us to assume that those CD169⁺ blebs may represent cell debris that emerges after cell death. However, we failed to detect perceptible signs of apoptosis along the subcapsular sinus floor in naive LNs with TUNEL staining. The positioning of CD169⁺ blebs within B-cell follicles also remained unaltered in mice lacking genes that encode proteins (Caspase-1, ASC, RIPK3 and MLKL) required for pyroptosis or necroptosis[29]. Furthermore, comparable amounts of CD169⁺ blebs were visualized even in germ-free mice devoid of PAMPs-expressing microbes (data not shown). Together with the observation of the much smaller size of the CD169⁺ blebs compared with that of typical apoptotic bodies, these results strongly indicate that the blebs are not shed by dead cells but rather are MVs actively secreted by SSMs. Indeed, various types of macrophages can release MVs to impact the microenvironment. Ravichandran et al. reported that the uptake of alveolar macrophage-derived MVs by airway epithelial cells could suppress inflammatory cytokine gene expression by the latter and protect against exacerbated lung inflammation after allergen exposure[30]. Studies from Li's lab and Ruf's lab showed that as

an essential initiator of coagulation, tissue factor (TF) release in the form of microvesicles from macrophages upon inflammasome activation leads to severe blood clotting and death of the host during sepsis[31, 32]. With regard to SSMs, Cyster's group reported the acquisition of CD169$^+$ blebs by IL7R^{hi}CCR6$^+$ innate-like lymphocytes based on the analysis of LN cell suspensions, although the possibility of blebs coming from SSM fragmentation during tissue preparation may exist[18, 33]. In our study, the in situ examination of LN sections by confocal imaging and correlative light and electron microscopy explicitly demonstrates the accumulation of SSM-derived CD169$^+$ MVs in follicles and, to the best of our knowledge, for the first time pinpoints the FDC network as one of the major targets. However, the mechanisms accounting for the preferential deposition on FDCs remain to be determined.

Within the GC area, the collaboration between antibody-producing B cells and the supportive stromal network jointly determines the quality of humoral responses. While a substantial body of studies have elucidated the molecular events governing GC B development, much less is known about FDC biology, especially the requirements for the regulation of their polarization. Only very limited reports are available regarding the molecular components involved in driving FDC maturation for them to acquire an LZ-related phenotype, including LTβR signaling[5, 34, 35], which is induced by B-cell-derived LTα1β2, and FcγRIIb-dependent signaling, which is initiated by IC trapped on the FDC surface[36]. Here, with imaging analysis and gene expression profiling, we found that CD169$^+$ MVs preferentially associate with LZ FDCs in both primary and secondary follicles. This selective association could be explained by two possibilities: elevated MV-binding ability of LZ FDCs or enhanced FDC maturation caused by CD169$^+$ MV deposition. Although we cannot completely exclude the first scenario, our data support the second scenario, as we could see decreased LZ-related gene expression in FDCs after ablation of CD169$^+$ MVs caused by long-term SSM depletion, in contrast to unchanged FDC maturation with short-term SSM depletion that leaves CD169$^+$ MVs intact. Future studies involving specific interference with CD169$^+$ MVs without SSM disruption would achieve a better understanding of the effect of CD169$^+$ MVs on FDCs. Nevertheless, our findings of selective LZ FDC targeting by SSM-derived MVs offer a novel perspective for the dissection of the mechanisms underlying FDC polarization, which is of critical importance in high-affinity antibody production.

MVs exert various functions in the immune system via the cargos they carry[37]. Despite the detailed molecular compositions in CD169$^+$ MVs awaiting further exploration, whether antigens could be transferred came into our focus, given that the long-term antigen depot on FDCs in the form of IC is an essential prerequisite for antibody affinity maturation during GC responses. In the current model, ICs circulated in lymph flow are first captured by SSMs, followed by transport via noncognate B cells in a complement receptor-dependent fashion, and eventually are deposited on the FDC network for presentation[27, 28]. The FDC targeting by SSM-derived CD169$^+$ MVs suggests an alternative antigen delivery route, paralleling the route mediated by B cells. The possible role of CD169$^+$ MVs as antigen carriers also fits the observation of their strong association with FDCs displaying a more activated phenotype because antigen-containing ICs have been reported to trigger FDC maturation[36]. Indeed, fluorescently tagged ICs could be detected on isolated CD169$^+$ MVs, and this colocalization was further confirmed in vivo. As our data demonstrate the possibility of CD169$^+$ MVs as carriers for antigen transport, the extent to which the MV-dependent route contributes to antigen deposition remains unclear. The experimental evaluation of this question requires specific blockade of SSM blebbing or interference with MV deposition while leaving SSMs intact and functional for antigen capture. However, based upon the imaging data showing a fraction of ICs interacting tightly with CD169$^+$ MVs, it is conceivable that CD169$^+$ MVs could play a complementary role in antigen delivery for an optimal GC response.

In conclusion, our study establishes a previously unrecognized MV-mediated intercellular connection between SSMs and the FDC network, with a potential effect in promoting FDC maturation. These findings may have important implications for vaccine design in terms of how the tight coordination between immune cells and the stromal network impacts the host response to infection.

Materials and methods

Mice

Wild-type mice with C57BL/6 background were purchased from Shanghai Laboratory Animal center (SLAC). CD169-DTR mice were generated as described previously[21] and purchased from RIKEN BRC (Cat$^{\#}$RBRC04395). LysM-Cre mice were originally from Jackson Laboratories (Cat$^{\#}$004781). Ms4a3-Cre mice and Rosa26-tdTomato mice were described previously[38]. Rosa26-tdTomato mice were bred with LysM-Cre mice and Ms4a3-Cre mice to obtain LysMCre-RosaTdT and Ms4a3Cre-RosaTdT mice, respectively. Six- to ten-week-old female mice were used for experiments unless noted otherwise.

Antibodies

For flow cytometry, cell sorting and immunofluorescence staining, the following antibodies were used: anti-CD45.2 (clone 104), anti-GP38 (clone 8.1-1), anti-CD31 (clone 390), anti-CD21/35 (clone 8D9; eBioscience), anti-CD169 (clone SER4; eBioscience), anti-CD169 (clone 3D6.112), rat IgG2a, κ isotype control antibody (clone RTK2758), anti-CD11b (clone M1/70), anti-CD11c (clone N418), anti-B220 (clone RA3-6B2), anti-CD3 (clone 17A2), anti-GL7 (clone GL7), anti-CD38 (clone 90), anti-CD16/32 (clone 2.4G2; BD Biosciences), anti-FDC-M1 (clone FDC-M1; BD Biosciences), anti-CD106 (clone 429), anti-CD23 (clone B3B4), anti-CD63 (clone NVG-2), anti-CD81 (clone Eat-2), Streptavidin, anti-Ki67 (clone 11F6), goat anti-rat IgG

(Invitrogen), DAPI (Invitrogen). All the antibodies used were purchased from BioLegend unless noted otherwise.

Immunofluorescence staining and confocal imaging

LNs were harvested and fixed overnight in 1% PFA, then dehydrated in 30% sucrose. Tissues were embedded in OCT freezing media (Sakura). 20 μm sections were prepared with a Leica cryostat and stained with indicated antibodies in standard staining buffer (PBS supplemented with 0.1 M Tris-HCl, 0.3% Triton X-100, 1% FBS, 1% BSA and 1% normal mouse serum, pH 7.4). Images were acquired on a Leica TCS SP8 confocal microscope or a Zeiss LSM-880 confocal microscope. Image processing and analysis were performed using Imaris software (Bitplane).

Voxel colocalization analysis was performed using the Coloc module of Imaris software. Briefly, the region of interest (ROI) was defined by generation of a mask for CD35 channel. Then, the intensity thresholds for CD35 channel and CD169 channel were set for colocalization analysis and the percentage of FDC volume colocalized with $CD169^+$ microvesicles was utilized for quantification of the colocalization.

Correlative light and electron microscopy

Freshly dissected lymph nodes were immediately transferred to freshly prepared fixation buffer containing 4% PFA and 0.03% glutaraldehyde for 40 min at room temperature (RT), embedded in 2% (w/v) low-melting point agarose (Sangon Biotech) in PBS. 50 μm sections were prepared with a Leica vibratome and placed in 35 mm glass bottom dishes for immunofluorescence staining. Images were acquired on a Leica TCS SP8 confocal microscope.

After the LM procedures, the samples were further fixed by immersion in 2.5% glutaraldehyde in 0.1 M phosphate buffer (pH 7.4) for 24 h at 4°C and washed in phosphate buffer. Samples were osmicated in 1% osmium containing 3% potassium ferricyanide (v/v) for 30 min at 4°C, incubated in 1% thiocarbohydrazide (TCH) (w/v) for 20 min at RT, followed by a second osmication in 1% osmium for 30 min at 4°C. Next, the samples were washed in ddH2O and incubated overnight in 1% aqueous uranyl acetate at 4°C. After final washing steps, the samples were then dehydrated stepwise through an ethanol series at 4°C, incubated in 50% epon resin for 2–3 h at RT, followed by an overnight incubation in 100% epon resin and subsequent embedding. Three-dimensional SEM was carried out using scanning electron microscope (GeminiSEM 300, Carl ZEISS), scanning 70 nm ultrathin sections over a distance of 6 μm.

Macrophage depletion

To deplete SSMs in CD169-DTR ($CD169^{DTR/+}$) mice, diphtheria toxin (DT; Merck) was injected intraperitoneally (20 ng/g). To locally deplete SSMs in popliteal LNs, 20 μl clodronate containing liposome (clodronate; Yeasen) or empty liposome (encapsome; Yeasen) were injected into the footpad (f.p.). The lymph nodes were harvested at time points as stated in the text for flow cytometry or immunofluorescence analysis.

Immunization

For multisite immunization, mice were subcutaneously injected with 75 μg keyhole limpet hemocyanin (KLH; Sigma) emulsified in complete Freund's adjuvant (CFA; Sigma) (300 μl each mouse). Immunization was administered at multiple sites near draining LNs (50 μl per site). 7 days post-immunization, draining inguinal lymph nodes, axillary lymph nodes and cervical lymph nodes were dissected for FDC isolation. For analysis of GC responses in popliteal lymphnode, mice were immunized with 10 μg KLH absorbed in 20 μl alum (Thermo Scientific) in each footpad. Draining popliteal lymph nodes were harvested 7 days post-immunization. Mice were immunized under isoflurane anesthesia.

Tissue preparation

Lymph nodes were digested for FDCs as described [39]. Briefly, lymph nodes were dissected, pierced with fine forceps in ice cold RPMI-1640. Then, the media was removed and replaced with freshly made enzyme mix containing 0.4 mg/ml Dispase® II (Cat# 4942078001; Roche), 0.2 mg/ml Collagenase P (Cat#11213865001; Roche) and 0.05 mg/mL DNase I (Cat#10104159001; Roche). Tubes were incubated in water bath for 50 min at 37°C until all the remaining lymph node fragments were completely digested. Digested cells were filtered through 70 μm cell strainers and lysed in ACK lysis buffer (ddH_2O supplemented with 155 mM NH_4Cl, 10 mM $KHCO_3$, 0.1 mM EDTA). Single cell suspensions were enriched for stromal cells by depleting $CD45^+$ hematopoietic cells using MACs microbeads (Miltenyi).

SSMs were isolated as described[28, 33]. Briefly, dissected lymph nodes were teased apart in freshly made enzyme mix containing 50 μg/ml Liberase TM (Cat#5401119001; Roche) and 0.05 mg/mL DNase I (Cat#10104159001; Roche). Tubes were incubated in water bath for 30 min at 37°C. The digestion reactions were quenched by the addition of 10% FBS and 5mM EDTA, and single cell suspensions were obtained using 70 μm cell strainers and syringe plungers.

Flow cytometry and cell sorting

Isolated cells were washed with FACs buffer (PBS supplemented with 2% FBS and 2mM EDTA) and nonspecific antibody binding was blocked by incubating cells with anti-CD16/32 for 15 min at 4°C. Cells were then stained with fluorophore-conjugated antibodies for 30 min at 4°C. Dead cells were excluded by Fixable Viability Stain 700 (BD Biosciences) staining. Intracellular staining

of CD169 was performed on surface-marked cells fixed and permeabilized with BD Cytofix/Cytoperm Kit (Cat# 554714) according to the manufacturer's instructions. Flow cytometry data were collected on a BD Fortessa X20 (BD Biosciences) and analyzed with FlowJo software (TreeStar). Fluorescence-activated cell sorting (FACS) was performed on a BD FACS Aria III (BD Biosciences) to achieve > 95% purity. The full gating strategies of our flow cytometry data are shown in supplementary Figure S5.

Quantitative Real-Time PCR (qRT-PCR)

Total RNA was extracted from sorted FDCs using the miRNeasy Micro Kit (Cat# 217084; QIAGEN) according to the manufacturer's instructions. Purified RNA was reversely transcribed into cDNA using the Hifair® II 1st Strand cDNA Synthesis SuperMix for qPCR (Cat#11123ES60; Yeasen), and qRT–PCR analysis using SYBR Green Real-time PCR Master Mix (Cat#QPK-201; TOYOBO) was performed on a ViiA7 Real-Time PCR System (Applied Biosystems). The following primers purchased from GENEWIZ were used for qRT–PCR:

Siglec1 forward primer 5'-CAGGGCATCCTCGACTGTC-3';
Siglec1 reverse primer 5'-GGAGCATCGTGAAGTTGGTTG-3';
Cr2 forward primer 5'-AACACATGGTTACCAGGTGTACC-3';
Cr2 reverse primer 5'-CGTGCCTCTCCAGCCATAAG-3';
Cxcl13 forward primer 5'-GGCCACGGTATTCTGGAAGC-3';
Cxcl13 reverse primer 5'-GGGCGTAACTTGAATCCGATCTA-3';
Cxcl12 forward primer 5'-TGCATCAGTGACGGTAAACCA-3';
Cxcl12 reverse primer 5'-TTCTTCAGCCGTGCAACAATC-3';
18S rRNA (18S ribosomal RNA) forward primer 5'-AGTCCCTGCCCTTTGTACACA-3';
18S rRNA (18S ribosomal RNA) reverse primer 5'-CGATCCGAGGGCCTCACTA-3'.

All data were normalized to *18S rRNA* quantified in parallel amplification reactions.

RNA-seq

Full-length cDNAs were generated with SMART-Seq® HT Kit (TAKARA) for library preparation and next-generation sequencing according to the manufacturer's protocol. Samples were sequenced on an Illumina NextSeq 500 sequencer, and the data were aligned to the mouse reference genome (version mm10). Differentially expressed genes (DEGs) identified by DESeq2 (adjusted P value < 0.05, fold change > 1.5) were used for gene ontology (GO) analysis.

Generation of immune complex in vivo

Mice were passively immunized with 2 mg polyclonal rabbit IgG anti-phycoerythrin (PE) (Cat#100-4199; Rocklands) intraperitoneally 12–16 h before subcutaneously injection of 10 μg R-phycoerythrin (Cat#2558; AAT Bioquest). 12 h after R-phycoerythrin injection, mice were sacrificed.

Enzymatic isolation of microvesicles from LNs

Lymph nodes were teased apart, digested with Liberase TM and DNase I as described above. PBS was added and cell suspensions were cooled down on ice for sequential ultracentrifugation. Briefly, the suspensions were centrifuged at 400 x g for 10 min, 2000 x g for 20 min to remove cells and large cell debris, respectively. The supernatants were then ultracentrifuged at 14000 x g for 35 min at 4°C to pellet microvesicles. Resuspended microvesicles were stained with fluorescently labeled antibody against CD169 for further analysis.

Statistical analysis

Statistical analysis was performed using GraphPad Prism, version 7.00 (GraphPad Software Inc.). Unpaired two-tailed Student's *t*-test was used for the statistical analysis of differences between two groups. One-way ANOVA was used for statistical analysis of multiple groups. Data are represented as mean ± s.e.m. and the exact P values are shown in each figure.

Acknowledgments: The authors thank Dr. Qiang Zou (Shanghai Institute of Immunology) for providing LysM-Cre mice, and Dr. Florent Ginhoux (Shanghai Institute of Immunology) for providing Ms4a3-Cre mice and Rosa26-tdTomato mice. This research was supported by the National Key Research and Development Program of China (No. 2021YFF0702100); the National Natural Science Foundation Projects of China (No. 31870871 and 32070901); Shanghai Science and Technology Commission (No. 22ZR1454600); General Financial Grant from the China Postdoctoral Science Foundation (No. 2018M632131 and 2018M632134); Shanghai Municipal Health Commission (No. 20204Y0118).

Conflict of interest: The authors declare no commercial or financial conflict of interests.

Author contributions: X.C. designed the study, performed most of the experiments, analyzed the data and wrote the manuscript; Y.Z. and S.L. performed experiments; W.Y. provided technical support; Z.L. designed the study, supervised the work and wrote the manuscript.

Ethics approval statement: All mice were maintained and bred in a specific pathogen-free animal facility in Shanghai Jiao

Tong University School of Medicine. All animal experiments were approved by the Institutional Animal Care and Use Committee (IACUC) of Shanghai Jiao Tong University School of Medicine and were performed in compliance with the University's guidelines for the care and use of laboratory animals.

Data availability statement: The RNA-seq data are available in the Sequence Read Archive (SRA) under accession number SRA: PRJNA841257. The data that support the findings of this study are available in the supplementary material of this article.

Peer review: The peer review history for this article is available at https://publons.com/publon/10.1002/eji.202249879

References

1 **Van den Broeck, W., Derore, A. and Simoens, P.**, Anatomy and nomenclature of murine lymph nodes: Descriptive study and nomenclatory standardization in BALB/cAnNCrl mice. *J Immunol Methods* 2006. **312**: 12-19.

2 **Mueller, S. N. and Germain, R. N.**, Stromal cell contributions to the homeostasis and functionality of the immune system. *Nat Rev Immunol* 2009. **9**: 618-629.

3 **Link, A., Vogt, T. K., Favre, S., Britschgi, M. R., Acha-Orbea, H., Hinz, B., Cyster, J. G. and Luther, S. A.**, Fibroblastic reticular cells in lymph nodes regulate the homeostasis of naive T cells. *Nat Immunol* 2007. **8**: 1255-1265.

4 **Kumar, V., Dasoveanu, D. C., Chyou, S., Tzeng, T. C., Rozo, C., Liang, Y., Stohl, W., Fu, Y. X., Ruddle, N. H. and Lu, T. T.**, A dendritic-cell-stromal axis maintains immune responses in lymph nodes. *Immunity* 2015. **42**: 719-730.

5 **Allen, C. D. C. and Cyster, J. G.**, Follicular dendritic cell networks of primary follicles and germinal centers: Phenotype and function. *Seminars in Immunology* 2008. **20**: 14-25.

6 **Mesin, L., Ersching, J. and Victora, G. D.**, Germinal Center B Cell Dynamics. *Immunity* 2016. **45**: 471-482.

7 **Pikor, N. B., Morbe, U., Lutge, M., Gil-Cruz, C., Perez-Shibayama, C., Novkovic, M., Cheng, H. W., Nombela-Arrieta, C., Nagasawa, T., Linterman, M. A., Onder, L. and Ludewig, B.**, Remodeling of light and dark zone follicular dendritic cells governs germinal center responses. *Nat Immunol* 2020. **21**: 649-659.

8 **Rodda, L. B., Bannard, O., Ludewig, B., Nagasawa, T. and Cyster, J. G.**, Phenotypic and Morphological Properties of Germinal Center Dark Zone Cxcl12-Expressing Reticular Cells. *J Immunol* 2015. **195**: 4781-4791.

9 **Asano, K., Kikuchi, K. and Tanaka, M.**, CD169 macrophages regulate immune responses toward particulate materials in the circulating fluid. *J Biochem* 2018. **164**: 77-85.

10 **Crocker, P. R., Hartnell, A., Munday, J. and Nath, D.**, The potential role of sialoadhesin as a macrophage recognition molecule in health and disease. *Glycoconjugate Journal* 1997. **14**: 601-609.

11 **O'Neill, A. S., van den Berg, T. K. and Mullen, G. E.**, Sialoadhesin - a macrophage-restricted marker of immunoregulation and inflammation. *Immunology* 2013. **138**: 198-207.

12 **Moseman, E. A., Iannacone, M., Bosurgi, L., Tonti, E., Chevrier, N., Tumanov, A., Fu, Y. X., Hacohen, N. and von Andrian, U. H.**, B cell maintenance of subcapsular sinus macrophages protects against a fatal viral infection independent of adaptive immunity. *Immunity* 2012. **36**: 415-426.

13 **Iannacone, M., Moseman, E. A., Tonti, E., Bosurgi, L., Junt, T., Henrickson, S. E., Whelan, S. P., Guidotti, L. G. and von Andrian, U. H.**, Subcapsular sinus macrophages prevent CNS invasion on peripheral infection with a neurotropic virus. *Nature* 2010. **465**: 1079-1083.

14 **Gonzalez, S. F., Lukacs-Kornek, V., Kuligowski, M. P., Pitcher, L. A., Degn, S. E., Kim, Y. A., Cloninger, M. J., Martinez-Pomares, L., Gordon, S., Turley, S. J. and Carroll, M. C.**, Capture of influenza by medullary dendritic cells via SIGN-R1 is essential for humoral immunity in draining lymph nodes. *Nat Immunol* 2010. **11**: 427-434.

15 **Gaya, M., Castello, A., Montaner, B., Rogers, N., Reis e Sousa, C., Bruckbauer, A. and Batista, F. D.**, Host response. Inflammation-induced disruption of SCS macrophages impairs B cell responses to secondary infection. *Science* 2015. **347**: 667-672.

16 **Junt, T., Moseman, E. A., Iannacone, M., Massberg, S., Lang, P. A., Boes, M., Fink, K., Henrickson, S. E., Shayakhmetov, D. M., Di Paolo, N. C., van Rooijen, N., Mempel, T. R., Whelan, S. P. and von Andrian, U. H.**, Subcapsular sinus macrophages in lymph nodes clear lymph-borne viruses and present them to antiviral B cells. *Nature* 2007. **450**: 110-114.

17 **Carrasco, Y. R. and Batista, F. D.**, B cells acquire particulate antigen in a macrophage-rich area at the boundary between the follicle and the subcapsular sinus of the lymph node. *Immunity* 2007. **27**: 160-171.

18 **Zhang, Y., Roth, T. L., Gray, E. E., Chen, H., Rodda, L. B., Liang, Y., Ventura, P., Villeda, S., Crocker, P. R. and Cyster, J. G.**, Migratory and adhesive cues controlling innate-like lymphocyte surveillance of the pathogen-exposed surface of the lymph node. *Elife* 2016. **5**.

19 **Barral, P., Polzella, P., Bruckbauer, A., van Rooijen, N., Besra, G. S., Cerundolo, V. and Batista, F. D.**, CD169(+) macrophages present lipid antigens to mediate early activation of iNKT cells in lymph nodes. *Nat Immunol* 2010. **11**: 303-312.

20 **Garcia, Z., Lemaitre, F., van Rooijen, N., Albert, M. L., Levy, Y., Schwartz, O. and Bousso, P.**, Subcapsular sinus macrophages promote NK cell accumulation and activation in response to lymph-borne viral particles. *Blood* 2012. **120**: 4744-4750.

21 **Miyake, Y., Asano, K., Kaise, H., Uemura, M., Nakayama, M. and Tanaka, M.**, Critical role of macrophages in the marginal zone in the suppression of immune responses to apoptotic cell-associated antigens. *J Clin Invest* 2007. **117**: 2268-2278.

22 **York, M. R., Nagai, T., Mangini, A. J., Lemaire, R., van Seventer, J. M. and Lafyatis, R.**, A macrophage marker, Siglec-1, is increased on circulating monocytes in patients with systemic sclerosis and induced by type I interferons and toll-like receptor agonists. *Arthritis Rheum* 2007. **56**: 1010-1020.

23 **Puryear, W. B., Akiyama, H., Geer, S. D., Ramirez, N. P., Yu, X., Reinhard, B. M. and Gummuluru, S.**, Interferon-inducible mechanism of dendritic cell-mediated HIV-1 dissemination is dependent on Siglec-1/CD169. *PLoS Pathog* 2013. **9**: e1003291.

24 **Zaborowski, M. P., Balaj, L., Breakefield, X. O. and Lai, C. P.**, Extracellular Vesicles: Composition, Biological Relevance, and Methods of Study. *Bioscience* 2015. **65**: 783-797.

25 **Uccini, S., Al-Jadiry, M. F., Pepe, G., Pasquini, A., Alsaadawi, A. R., Al-Hadad, S. A., Di Napoli, A., Tripodo, C. and Ruco, L.**, Follicular dendritic cells display microvesicle-associated LMP1 in reactive germinal centers of EBV+ classic Hodgkin lymphoma. *Virchows Arch* 2019. **475**: 175-180.

26 **Bajenoff, M. and Germain, R. N.**, B-cell follicle development remodels the conduit system and allows soluble antigen delivery to follicular dendritic cells. *Blood* 2009. **114**: 4989-4997.

27 **Phan, T. G., Grigorova, I., Okada, T. and Cyster, J. G.**, Subcapsular encounter and complement-dependent transport of immune complexes by lymph node B cells. *Nat Immunol* 2007. **8**: 992-1000.

28 **Phan, T. G., Green, J. A., Gray, E. E., Xu, Y. and Cyster, J. G.**, Immune complex relay by subcapsular sinus macrophages and noncognate B cells drives antibody affinity maturation. *Nat Immunol* 2009. **10**: 786-793.

29 **Bertheloot, D., Latz, E. and Franklin, B. S.**, Necroptosis, pyroptosis and apoptosis: an intricate game of cell death. *Cell Mol Immunol* 2021. **18**: 1106-1121.

30 **Han, C. Z., Juncadella, I. J., Kinchen, J. M., Buckley, M. W., Klibanov, A. L., Dryden, K., Onengut-Gumuscu, S., Erdbrugger, U., Turner, S. D., Shim, Y. M., Tung, K. S. and Ravichandran, K. S.**, Macrophages redirect phagocytosis by non-professional phagocytes and influence inflammation. *Nature* 2016. **539**: 570-574.

31 **Wu, C., Lu, W., Zhang, Y., Zhang, G., Shi, X., Hisada, Y., Grover, S. P., Zhang, X., Li, L., Xiang, B., Shi, J., Li, X. A., Daugherty, A., Smyth, S. S., Kirchhofer, D., Shiroishi, T., Shao, F., Mackman, N., Wei, Y. and Li, Z.**, Inflammasome Activation Triggers Blood Clotting and Host Death through Pyroptosis. *Immunity* 2019. **50**: 1401-1411.e1404.

32 **Rothmeier, A. S., Marchese, P., Petrich, B. G., Furlan-Freguia, C., Ginsberg, M. H., Ruggeri, Z. M. and Ruf, W.**, Caspase-1-mediated pathway promotes generation of thromboinflammatory microparticles. *J Clin Invest* 2015. **125**: 1471-1484.

33 **Gray, E. E., Friend, S., Suzuki, K., Phan, T. G. and Cyster, J. G.**, Subcapsular Sinus Macrophage Fragmentation and CD169(+) Bleb Acquisition by Closely Associated IL-17-Committed Innate-Like Lymphocytes. *Plos One* 2012. **7**.

34 **Kranich, J. and Krautler, N. J.**, How Follicular Dendritic Cells Shape the B-Cell Antigenome. *Front Immunol* 2016. **7**: 225.

35 **Fu, Y. X. and Chaplin, D. D.**, Development and maturation of secondary lymphoid tissues. *Annu Rev Immunol* 1999. **17**: 399-433.

36 **El Shikh, M. E., El Sayed, R., Szakal, A. K. and Tew, J. G.**, Follicular dendritic cell (FDC)-FcgammaRIIB engagement via immune complexes induces the activated FDC phenotype associated with secondary follicle development. *Eur J Immunol* 2006. **36**: 2715-2724.

37 **Robbins, P. D. and Morelli, A. E.**, Regulation of immune responses by extracellular vesicles. *Nat Rev Immunol* 2014. **14**: 195-208.

38 **Liu, Z., Gu, Y., Chakarov, S., Bleriot, C., Kwok, I., Chen, X., Shin, A., Huang, W., Dress, R. J., Dutertre, C. A., Schlitzer, A., Chen, J., Ng, L. G., Wang, H., Liu, Z., Su, B. and Ginhoux, F.**, Fate Mapping via Ms4a3-Expression History Traces Monocyte-Derived Cells. *Cell* 2019. **178**: 1509-1525 e1519.

39 **Fletcher, A. L., Malhotra, D., Acton, S. E., Lukacs-Kornek, V., Bellemare-Pelletier, A., Curry, M., Armant, M. and Turley, S. J.**, Reproducible isolation of lymph node stromal cells reveals site-dependent differences in fibroblastic reticular cells. *Frontiers in Immunology* 2011. **2**.

Abbreviations: **LNs**: lymph nodes · **FDCs**: follicular dendritic cells · **SSMs**: subcapsular sinus macrophages · **MVs**: microvesicles · **LZ**: light zone · **DZ**: dark zone · **ICs**: immune complexes · **GC**: germinal center · **ROI**: region of interest · **CLEM**: correlative light and electron microscopy · **PE**: phycoerythrin

Full correspondence: Dr. Zhiduo Liu, Shanghai Institute of Immunology, 280 South Chongqing Road, Huangpu District, Shanghai, 200013, China, Email: zhiduo.liu@shsmu.edu.cn

Received: 28/2/2022
Revised: 21/7/2022
Accepted: 29/7/2022
Accepted article online: 30/7/2022